Drift of elastic floating ice sheets by waves and current, part I

Kostikov, V.; Hayatdavoodi, M.; Ertekin, R. C.

Published in:
Proceedings of the Royal Society A: Mathematical, Physical and Engineering Sciences

Publication date:
2021

Document Version
Peer reviewed version

Citation for published version (APA):
Kostikov, V., Hayatdavoodi, M., & Ertekin, R. C. (2021). Drift of elastic floating ice sheets by waves and current, part I: single sheet. *Proceedings of the Royal Society A: Mathematical, Physical and Engineering Sciences*, *477*(2254).

PROCEEDINGS A

rspa.royalsocietypublishing.org

Research

Article submitted to journal

Subject Areas:
applied mathematics, fluid mechanics, oceanography, ocean engineering, wave motion

Keywords:
wave-induced drift, wave-current loads, hydroelasticity, nonlinear wave-structure interaction, deformable ice sheets, Green-Naghdi equations

Author for correspondence:
M. Hayatdavoodi
e-mail:
m.hayatdavoodi@dundee.ac.uk

Drift of elastic floating ice sheets by waves and current, part I: single sheet

V. Kostikov[1], M. Hayatdavoodi[1,2] and R. C. Ertekin[1,3]

[1] College of Shipbuilding Engineering, Harbin Engineering University, Harbin, China
[2] School of Science and Engineering, University of Dundee, DD1 4HN, UK
[3] Ocean & Resources Engineering Department, University of Hawaii, Honolulu, HI 96822, USA

The drift motion of a freely floating deformable ice sheet in shallow water subjected to incident nonlinear waves and uniform current is studied by use of the Green-Naghdi theory for the fluid motion and the thin plate theory for an elastic sheet. The nonlinear wave- and current-induced forces are obtained by integrating the hydrodynamic pressure around the body. The oscillations and translational motion of the sheet are then determined by substituting the flow-induced forces into the equation of motion of the body. The resulting governing equations, boundary and matching conditions are solved in two-dimensions with a finite difference technique. The surge and drift motions of the sheet are analyzed in a broad range of body parameters and various wave-current conditions. It is demonstrated that wavelength to sheet length ratio plays an important role in the drift response of the floating sheet, while the sheet mass and rigidity have comparatively less impact. It is also observed that while the presence of the ambient current changes the drift speed significantly (almost linearly), it has little to no effect on it's oscillations. However, under the same ambient current, the drift speed changes remarkably by the wave period (or wavelength).

An object floating freely on the ocean surface drifts as a result of combined action of waves, currents and wind. The drift motion is typically accompanied by oscillations at the frequencies of the incident wave. To the author's knowledge, this is one of the first studies on nonlinear wave- and current- induced drifting motions of floating ice sheets, particularly in shallow waters.

THE ROYAL SOCIETY PUBLISHING

1. Introduction

As a result of global warming, larger areas of the ocean surface in polar regions are being released from ice in summertime [1]. This stimulates the development of Northern sea routes and facilitates the mining operations there. At the interface between open waters and frozen ocean, there are marginal ice zones (MIZ) consisting of the ice floes of different sizes and shapes, which on interaction with ocean waves and currents may drift towards moving vessels or stationary offshore structures [2]. Ice floes in the MIZ can be extremely mobile with instantaneous drift speed of as large as 0.75 m/s in storm conditions [3]. The hazards of the drifting ice to offshore and shipping operations can be estimated by proper description of wave- and current-induced ice motions. This would allow prediction of the velocity of the travelling ice and the dispersal rates for groups of floating ice objects of different sizes. Mutual collisions and vertical stacking (rafting) of the ice floes are thought to be the source of both floe destruction and composite ice formation [4]. Ice floes increase in diameter and thickness as a result of periodical wave action, pushing the individual ice floes into composite ice formations [5]. Thus, in addition to melting, surface waves play a determining role in forming the shape of MIZ. In view of this, it is of interest to understand the principles of wave and current interactions with the ice sheets and other floating objects prior to collision.

As it is evident from the above, there is need for developing models capable of describing the drift response of floating deformable objects to incident waves and currents. The process of transport of fluid particles by waves is known as «Stoke's drift» [6], and in the absence of the floating body is quite well understood, but theoretical studies on the subject of wave and current-induced drift of floating objects are extremely rare. The development in this field so far is limited mainly to the case of small rigid bodies and linear potential flows.

Historically, the problem of interaction between the fluid and floating rigid bodies has been solved theoretically by perturbation expansions methods with a small parameter [7,8], or numerically by the finite element method (FEM) or boundary element method (BEM) [9,10]. In a classic survey on motion of floating bodies by Wehausen [11] the general equations governing the motion of a floating rigid body in regular and irregular waves with the linear theory framework were presented. Apart from the linear wave force responsible for the major part of wave loading, there is nonlinear force components, giving rise to an actual drift of the body. Faltinsen & Locken [7] solved the boundary-value problem to the second order in wave amplitude and calculated the necessary slow drift excitation forces. Two different approaches to calculate the horizontal force exist, namely, the near-field and far-field methods. The near-field method is based on direct integration of all contributors to the second-order force over the instantaneous wetted surface of the floating structure. In the far-field method, the drift force is obtained from the linear momentum flux at infinity. Grue and Palm [12] used both near- and far-field formulas for calculation of the drift forces on a ship in waves with and without current. Chen [13] showed the equivalence of both approaches and combined them to derive the middle-field approach for calculation of the second-order wave loads.

The most commonly used approach to describe the drift motion of ice floes in waves is the slope-sliding model. In this model, originally proposed by Rumer *et al.* [14] and further developed in subsequent works [5], [15–17], the wave is simplified as a slope along which the floe can slide under the action of gravity without disturbing the wave field. This model is based on modified Morison's equation, valid for slender floating bodies. It suggests that, when wavelength is much longer than dimensions of the body, the wave diffraction is negligible. For wavelengths less than two floe diameters, as to Meylan et al. [16], an alternative method is required.

In order to track the moving fluid-solid contact surface and thereby describe the motion of a freely floating body, adaptive moving mesh (a.k.a. dynamic mesh) methods are required. In adaptive schemes, the grid used in calculations does not depend on the location of the body relative to the surrounding fluid. Such a grid makes the computation of nonlinear problems with the two-way fluid moving body interaction more efficient than conventional approaches. For example, in the Constrained Interpolation Profile method (CIP) the fluid-body interaction is treated as a multi-phase problem, which has liquid, gas and solid phases, modelled numerically by one set of hydrodynamic equations on a nonuniform staggered Cartesian grid [18]. The moving boundaries are distinguished by a density function. In Smoothed Particle Hydrodynamics method (SPH), a Lagrangian approach, the fluid medium is represented as a collection of separate particles interacting with each other and with the solid body [19]. These fluid particles transport mass, momentum and energy as they move inside the computational domain. In principle, the meshless character of the SPH-based methods allows to treat the free motions of a body inside the fluid domain in an easier way with respect to the mesh-based solvers and thereby are appropriate for description of simultaneous motions of constantly changing free surface and solid boundaries. In spite of the ability to model strongly nonlinear wave-body interaction problems accurately, SPH-based models are time-consuming and require high computational powers.

If ocean waves have wavelength much larger than the ice thickness, as discussed by Weber [20], the ice can be treated as a layer of viscous Newtonian fluid. Using the Lagrangian formulation, Weber [20] described the displacement and pressure fields in the viscous layer in terms of expansions with wave amplitude as a small parameter. Under the same assumption, Law [21] utilized the conformal mapping for a series of progressive waves propagating under an inextensible thin film and produced the estimation for the drift velocity, caused by combined shear stresses and pressure force.

To date, despite the development of some numerical models and laboratory investigations of floe response in waves, to the authors' knowledge, no approach is developed to study interaction of nonlinear waves and currents with drifting elastic structures in waters of finite depth which are large enough to modify the flow field. The present study is the first attempt to build theoretical model of wave- and current-induced drift of an elastic plate of arbitrary length, elasticity and thickness and provide insight about the fluid and structure dynamics. In our recent work [22], we have considered the interaction of nonlinear waves with a set of elastic plates, restricted to the vertical motion. In this paper, we will study wave and current interaction with a floating elastic sheet, which is free to drift horizontally.

The outline of the remaining of the paper is as follows. Firstly, the methodology, including the model description, governing equations, boundary conditions, determination of the horizontal forces, and numerical calculation method are presented. Then, the constructed model is tested first by comparing with the available data and then by performing the analysis with various elastic sheets and incoming waves and current conditions. Finally, some conclusions are made based on the model performance and obtained results. Analysis of any model involving multiple structures should start with the analysis of a single object. Therefore, the focus of the part I of this study will be on the single elastic sheet, and the part II shall be dedicated to the case of multiple sheets.

2. Mathematical formulation

An elastic sheet of length L, thickness δ, mass per unit width m, draft d, and flexural rigidity D is floating freely on the surface of an inviscid fluid of constant density ρ and depth h (figure 1). The sheet is initially at rest and is free to move horizontally with respect to the stationary seafloor. The Cartesian reference frame will be used in which the x axis is pointing to the right, y axis is directed upwards, and its origin is situated on the undisturbed free surface. Nonlinear incident waves of height H and length λ (or period T), created by the wavemaker, propagate in the positive x–direction and interact with the floating sheet. Uniform current is also generated by the wavemaker (here wave- and current-maker) and may be faworable (in positive x direction) or adverse.

It is assumed that the elastic sheet is directly in touch with the fluid at all times and the friction at the contact surface is negligible. Overwash, formation of air gaps, cracks and jets are excluded from the fluid-sheet interaction process. In a recent study on overwash by [23], it is found that the fluid spilling onto the upper surface of the sheet has an impact on responses in terms of

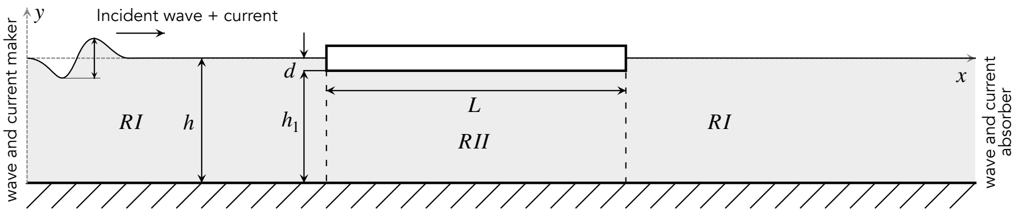

Figure 1. Schematic of the problem of waves and current interaction with a deformable surface on top, and the two fluid regions referred to in the text.

deflection amplitudes, energy dissipation and wave transmission. The same group of authors reported earlier [24] that drifting plates experience less overwash than the plates with mooring.

The depth of the fluid under the sheet at rest is $h_1 = h - d$. The equations are formulated and the results are presented in dimensionless form after using ρ, h and g as a dimensionally independent set, where g is the acceleration due to gravity. It should be noted that the magnitudes of dimensionless unit mass m and dimensionless draft d are equal. Henceforth, all variables, unknown functions and parameters are dimensionless unless otherwise stated.

(a) The Green-Naghdi equations

The mathematical formulation of wave interaction with an elastic sheet is based on the nonlinear Level I Green-Naghdi (GN) theory. The GN theory was originally developed by Green & Naghdi [25,26] from the theory of directed fluid sheets for any type of incompressible medium. In the absence of any perturbation and scaling restrictions, the GN equations satisfy the nonlinear boundary conditions exactly, while the integrated mass and momentum conservation laws are postulated. In the Level I GN theory, utilized in this study, a linear distribution of the vertical velocity along the water column is assumed, which leads to horizontal velocity being invariant over the water column. Hence, the Level I GN equations are applicable to propagation of long waves in shallow water.

Note that irrotationality of the flow is not a requirement in general, although this assumption can be made and would result in an special version of the equations known as the Irrotational Green-Naghdi Equations (IGN), see [27,28] for derivations of the IGN theory, and [29,30] for some applications (including comparisons of IGN results of variable levels with Level I GN equations utilized here). High-level GN equations, generally applicable to nonlinear, unsteady flow motion in any water depths, can be obtained by assuming higher order polynomials (or, alternatively, exponential functions) for the vertical velocity distribution over the water column. Further discussion on the High-level GN equations can be found in [31–34].

In the analysis of this problem, it becomes necessary to divide the domain into regions of two types. On the top of Region I (RI) there is a free surface, where the fluid pressure is constant atmospheric pressure, and the surface tension is negligible. On the top of Region II (RII) there is an elastic plate, where, as opposed to Region I, the fluid pressure is variable. Regions RI and RII are connected through discontinuity lines going vertically from the plate edges to the bottom.

The basic equations governing the fluid motion in RI are provided by the Level I GN theory for a flat and stationary seafloor and zero top pressure, written in dimensionless form as [35]:

$$\eta_{,t} \quad + \quad (1+\eta)u_{,x} + u\eta_{,x} = 0, \tag{2.1}$$

$$3\dot{u} \quad + \quad 3\eta_{,x} + 2\eta_{,x}\ddot{\eta} + (1+\eta)\ddot{\eta}_{,x} = 0, \tag{2.2}$$

for the unknown horizontal fluid velocity $u(x,t)$ and free surface elevation $\eta(x,t)$, measured from the still water level. Subscripts after comma denote partial derivatives with respect to the given variable and upper dot specifies the total time (or material) derivative. Note that equations (2.1) and (2.2) are statements of conservation of mass and linear momentum, respectively. The same way, the governing equations for the fluid flow under elastic sheets in RII is formulated as:

$$\zeta_{,t} \quad + \quad (h_1+\zeta)u_{,x} + u\zeta_{,x} = 0, \tag{2.3}$$

$$3\dot{u} \quad + \quad 3\zeta_{,x} + 3\hat{p}_{,x} + 2\zeta_{,x}\ddot{\zeta} + (h_1+\zeta)\ddot{\zeta}_{,x} = 0, \tag{2.4}$$

where $\zeta(x,t)$ is elastic deformation of the sheet, measured from its stationary position. The fluid pressure at the fluid-structure contact surface $\hat{p}(x,t)$ is coupled with the structural elasticity by the thin plate theory [36]:

$$\hat{p} - m(1+\zeta_{,tt}) - D\zeta_{,xxxx} = 0, \tag{2.5}$$

where the flexural rigidity is defined by

$$D = \frac{E\delta^3}{12(1-\nu^2)}, \tag{2.6}$$

with δ, E and ν being the thickness, Young's modulus and Poisson's ratio of the sheet, respectively. Note that formula (2.5) for the elastic plate can be modified to include extra terms, e.g. compressive stress which is proportional to the second derivative of the plate deformation ζ_{xx}. Barman et al. demonstrated that in the presence of compression, the group velocity of hydroelastic wave under certain conditions goes to zero, i.e. wave blocking can occur under such conditions, see [37].

Ertekin [38] derived the explicit relations for the vertical velocity along the water column:

$$v(y) = \dot{\eta}(1+y)/(1+\eta), \quad \text{in} \quad RI, \qquad v(y) = \dot{\zeta}(1+y)/(h_1+\zeta) \quad \text{in} \quad RII, \tag{2.7}$$

and pressure on the bottom $y=-1$:

$$\bar{p} = \frac{1}{2}(1+\eta)(\ddot{\eta}+2) \quad \text{in} \quad RI, \qquad \bar{p} = \frac{1}{2}(h+\zeta)(\ddot{\zeta}+2) \quad \text{in} \quad RII, \tag{2.8}$$

which can be written both under the free surface in region RI and under the sheet in region RII. Pressure distribution in both regions can be obtained from Euler's equation in the form [22]:

$$p(x,y) = \begin{cases} \frac{1}{2}(1+\eta)(\ddot{\eta}+2) - (y+1) - \frac{1}{2}(y+1)^2\ddot{\eta}/(1+\eta), & (x,y) \in RI \\ \frac{1}{2}(h_i+\zeta)(\ddot{\zeta}+2) + \hat{p} - (y+1) - \frac{1}{2}(y+1)^2\ddot{\zeta}/(h_1+\zeta), & (x,y) \in RII. \end{cases} \tag{2.9}$$

Vertical velocity $v(y)$ and pressure $p(x,y)$ are not involved in constitutive equations (2.1)–(2.4) and therefore can be found analytically from relations (2.7)–(2.9), once the solution η, ζ and u are known. For detailed analysis of the fluid velocity and pressure fields under collection of elastic plates the reader is referred to [22].

(b) The boundary, matching and jump conditions

Equations (2.1)–(2.4) already include the exact nonlinear kinematic and dynamic boundary conditions at the free surface $y=\eta(x,t)$ and fluid-structure contact surfaces $y = \zeta(x,t)$, as well as the impermeability condition on the bottom $y=-1$. For a continuous solution throughout the domain, it is necessary to connect the solutions obtained in each region through proper boundary and matching conditions at the interfaces dividing the regions. Since an ice sheet can drift under the action of waves and current, the horizontal coordinates of the leading and trailing edges x^L and x^T are not fixed. The edges as well as all points of the sheet undergo the same drift motion with velocity $U(t)$, so that any possible deformation occurring in the sheet is limited to the vertical bending. At the edges of a freely floating sheet, bending moments and shear stresses should be zero, i.e.,

$$\zeta_{,xx} = 0, \qquad \zeta_{,xxx} = 0 \qquad (x = x^L, \quad x = x^T). \tag{2.10}$$

Moreover, by assumption, the sheet is always in contact with the fluid, so that no air gaps are allowed. Therefore, the mass continuity equation (2.3), valid throughout the domain, together with condition (2.10) imply:

$$3\zeta_{,x}u_{,xx} + (h_i+\zeta)u_{,xxx} = 0 \qquad (x=x^L, \quad x=x^T), \tag{2.11}$$

$$4\zeta_{,x}u_{,xxx} + (h_i+\zeta)u_{,xxxx} + \zeta_{,xxxx}(u-U) = 0 \qquad (x=x^L, \quad x=x^T). \tag{2.12}$$

The presence of elastic surface with non-zero draft causes jumps in the fluid layer thickness throughout the flow domain. This leads to discontinuity of fluid particle velocity $u(x,t)$ and its derivatives at the interfaces between regions. Under such conditions, the theory demands for appropriate jump conditions to ensure continuity of mass, momentum and energy (in general) across the discontinuity curves, see [39–43] for derivations of the jump conditions of the GN equations as applied to a number of problems. See Hayatdavoodi and Ertekin [44] for a derivation of the jump conditions for nonlinear wave interaction with a thin plate by the Level U GN equations (as applied here).

Moreover, the physics of the problem demands the continuity of mass flux across the discontinuity curves between the regions, formulated as follows:

$$\eta(u-U)|_{x^L-0} = \zeta(u-U)|_{x^L+0}, \qquad \zeta(u-U)|_{x^T-0} = \eta(u-U)|_{x^T+0}. \tag{2.13}$$

Here, $x^L \pm 0$ and $x^T \pm 0$ denote the single-sided limiting values of x^L and x^T, respectively. In equation (2.13), the instantaneous drift speed of the sheet U is subtracted from the limiting values of horizontal fluid velocity at the edges, to account for the moving boundaries. We also require continuous bottom pressure $\bar{p}$ across the discontinuity curves, which is evaluated from equation (2.8), across the interfaces between the regions, i.e.,

$$\frac{1+\eta}{2}(\ddot{\eta}+2)|_{x^L-0} = \frac{h_1+\zeta}{2}(\ddot{\zeta}+2)|_{x^L+0} + \hat{p}|_{x^L+0}, \tag{2.14}$$

$$\frac{h_1+\zeta}{2}(\ddot{\zeta}+2)|_{x^T-0} + \hat{p}|_{x^T-0} = \frac{1+\eta}{2}(\ddot{\eta}+2)|_{x^T+0}. \tag{2.15}$$

On the left side of the domain, a numerical wave- and current-maker generates periodic nonlinear waves (cnoidal waves), satisfying the GN equations (2.1)–(2.2), and uniform current, when required. Derivation of the periodic shallow-water wave solution of the Level I GN equations can be found in [45]. The combined action of wave and current of constant speed U_c is determined by specifying the horizontal velocity at the wavemaker as:

$$u_c(x-ct) = \frac{c\cdot\eta(x-ct)}{1+\eta(x-ct)} + U_c, \tag{2.16}$$

where η is the cnoidal wave solution at the wavemaker and c is the constant phase speed of the wave. On the right side of the domain, the open-boundary Orlanski's condition is prescribed to reduce reflections back into the wave tank:

$$\eta_{,t} \pm c\eta_{,x} = 0, \quad u_{,t} \pm cu_{,x} = 0. \tag{2.17}$$

Initially, the fluid is either at rest or flows with the speed of the current U_c:

$$\eta(x,0)=0, \quad u(x,0) = \begin{cases} 0, & \text{waves-only cases} \\ U_c, & \text{waves \& current combined.} \end{cases} \tag{2.18}$$

Supplemented by boundary and initial conditions (2.10)–(2.18), equations (2.1)–(2.5) represent a set of coupled, nonlinear partial differential equations that may be solved for unknowns $\eta(x,t)$, $\zeta(x,t)$, $u(x,t)$ and $\hat{p}(x,t)$. The number of unknowns, however, is one more than the number of equations. The system of equations is closed by considering the equation of motion of the ice sheets.

(c) Drift motion of the sheet

In the absence of collisions, the drift motion of floating sheets due to hydrodynamic pressure forces is determined by solving Newton's second law. Hence, the translational motion of the center of mass of the floating sheet, including its horizontal velocity U and coordinate X, is determined through:

$$mL\frac{dU}{dt} = F(t), \qquad \frac{dX}{dt} = U(t). \tag{2.19}$$

Following the near-field approach, the horizontal projection of hydrodynamic pressure force F is calculated by integrating the fluid pressure along the fluid-sheet contact surface $y = \zeta(x,t)$, from the leading edge to the trailing edge, and taking the horizontal component of the resulting pressure force, i.e.,

$$F(t) = -\int_{x^L}^{x^T} \hat{p}(x,t)\zeta_{,x}dx + f(t). \tag{2.20}$$

The term $f(t)$ in formula (2.20) denotes the horizontal force on to the edges of the sheet. Since the sheet is immersed into the fluid and has non-zero draft, the pressure differential of the edges of the sheet contribute to the total horizontal force. In view of the shallow water conditions and thinness of the sheet, we assume linear distribution of hydrodynamical pressure across the edges of the sheets (see [22,46,47] for discussion on vertical pressure distribution under Level I GN equations). Hence, pressure varies from $\hat{p}$ at the bottom edges of the sheet bottom surface to zero on the free surface. The force associated to the leading and trailing edge pressure differentials f is given as

$$f(t) = \frac{\hat{p}(x^L,t)}{2}\left[\eta(x^L,t) - \zeta(x^L,t) + d\right] - \frac{\hat{p}(x^T,t)}{2}\left[\eta(x^T,t) - \zeta(x^T,t) + d\right]. \tag{2.21}$$

There may be difference between surface elevation and plate deformation at the edges. But if to take the SWL as the reference, the term $f(t)$ can be approximated by:

$$f(t) = \frac{1}{2}\left[\hat{p}(x^L,t) - \hat{p}(x^T,t)\right] d. \tag{2.22}$$

The wave reflection occurs due to the passage from region RI to region RII, characterized by different thickness of the fluid layer and pressure on top. The friction forces associated with the disposition of the sheets relative to the fluid are assumed negligible when compared with the wave-induced force. Note, that integration limits x^L, x^T, as well as the integrand $\hat{p}(x,t)$ change with time. Hence equations (2.19)–(2.20) are coupled with the system (2.1)–(2.5) through the drift motion and should be solved simultaneously for the unknowns.

(d) Numerical solution

The computational procedure consists of the following recurring blocks. First, the free surface elevation $\eta(x,t)$ in Regions RI and sheets deformations $\zeta(x,t)$ in Regions RII are calculated from equations (2.1) and equations (2.3), respectively. Then, the horizontal velocity $u(x,t)$ is calculated from momentum equations (2.2) and (2.4), subjected to the boundary and matching conditions (2.12)–(2.15). The structure of governing equations allows to eliminate the time derivatives of η and ζ from momentum equations (2.2) and (2.4), so that unknown functions can be evaluated independently at each time step, see [38] for more details. In spatial discretization, we use the second-order accurate central-difference formulas for derivatives, and for marching in time we employ the explicit modified Euler's method. Momentum equations (2.2) and (2.4) are finally reduced to a set of linear equations with a banded matrix, which is solved by the Gaussian Elimination algorithm. For further details about the discretization and matrix evaluation the reader is referred to [44], where a similar numerical scheme has been successfully applied to the problem of wave interaction with a submerged rigid plate.

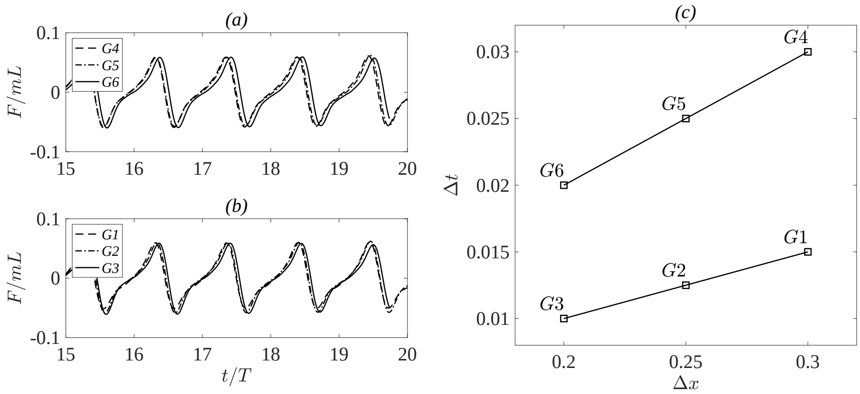

Figure 2. (a,b) Time history of horizontal force on a freely floating sheet ($L=3$, $m=0.1$, $D=1$) under the action of a cnoidal wave ($\lambda/L=5$, $H=0.2$) without current, obtained by use of (c) different grids.

The horizontal position X of the drifting sheet changes with time, as it depends on direction, duration and magnitude of the wave forcing, according to equation (2.19). The sheet is assumed inextensible in horizontal direction, and the unknown X can denote any point on the sheet: leading edge x^L, trailing edge x^T, or its center of mass, differing by a constant. The numerical integration of equations (2.19) is implemented by the two-step modified Euler's method as follows:

$$U^{\overline{n+1}} = U^n + \frac{F^n}{mL}\Delta t, \qquad X^{\overline{n+1}} = X^n + U^n \Delta t, \tag{2.23}$$

$$U^{n+1} = U^n + \frac{1}{2}\frac{F^n + F^{\overline{n+1}}}{mL}\Delta t, \qquad X^{n+1} = X^n + \frac{1}{2}(U^{n+1} + U^{\overline{n+1}})\Delta t, \tag{2.24}$$

where n is the time iteration index, Δt is the time step and superscript $\overline{n+1}$ indicates the results at the middle step. Thus, knowing the previous position X^n, instantaneous velocity U^n and horizontal force F^n, the new position of the sheet X^{n+1} can be determined.

In our formulation, there is no gap between the fluid and the floating sheet at all times. Therefore, the position and length of regions RI and RII may change with horizontal motion of the sheet. In the present numerical scheme, the location of discontinuity curves between regions are updated repeatedly according to relations (2.23) and (2.24). Since we use uniform mesh, the change in the location of the boundaries occurs when horizontal displacement of the sheet X exceeds the size of the grid Δx. Hence, we take Δx sufficiently small to ensure that motions, however small, are captured; this will be revisited in the following sections. To ensure the continuity of surface elevation and fluid particle velocity in the open water Regions RI during the relocation process, the calculated solution is redistributed inside the inner nodes using the linear interpolation formula.

The effect of space and time discretization, as well as their ratio, is studied by the convergence of the solution shown in figure 2. The results obtained through different mesh configurations are very close, yet with a finer space discretization, the differences between the calculated results tend to be even smaller, which implies the numerical convergence of the scheme. Figure 2 implies that even though the horizontal motion of the sheet can be of a smaller scale than the spatial grid size, this has a negligible effect on the final solution. In subsequent sections, we will use the grid $G3$ as the converged mesh, which is optimal for the current problem regarding the accuracy and calculation time.

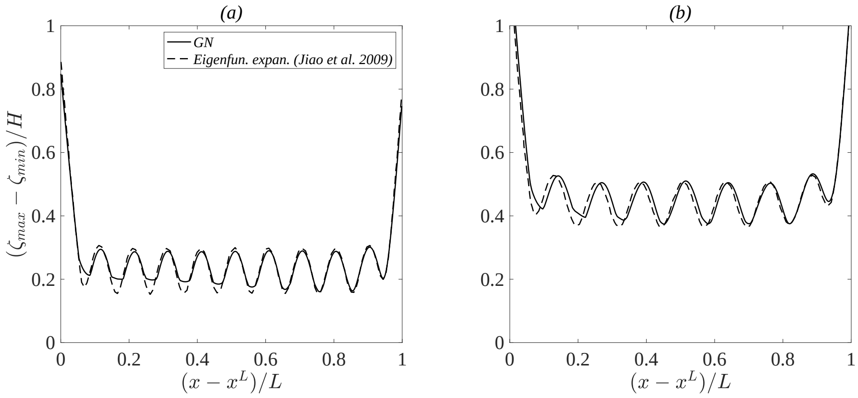

Figure 3. Comparisons of deformation heights of the sheet ($L = 60$, $m = 0.05$, $D = 28.5$) under the action of regular waves of lengths (a) $\lambda/L = 0.1$ and (b) $\lambda/L = 0.18$ without current.

3. Comparisons with experiments and alternative models

Validation of the results obtained in this study is difficult due to the lack of experimental data and numerical calculations in the field. Existing experimental works with unconstrained drift are mostly confined to studies with polyethylene plates of extremely small size [48,49]. This is justified by an assumption that small plates, having comparable thickness and length dimensions, behave as rigid bodies and thus their flexural response can be neglected. Many numerical calculations were also conducted with short-sized plates, because in underlying theoretical models small plate length to wavelength ratio was required in order to eliminate the effect of the floating plate on the incident wave [5,16,17]. The numerical study on the drift of long elastic sheets of Watanabe et al. [50] was conducted for infinite water depth condition and is not applicable to this study.

Therefore, for comparison purposes, we initially examine the hydroelastic behaviour of various floating sheets in different wave conditions without current, restrained from moving horizontally, and focus on the performance of the model in determining the elastic deformations. Figures 3 and 4 compare the deflection amplitudes at each point of the sheet predicted by the GN equations and calculated by eigen-expansion method [8,10]. Comparisons are normalized with respect to the wave height H, and the horizontal coordinate is normalized with respect to the sheet length L. Figures 3 and 4 illustrate that the deformation increases significantly near the edges of the sheet and varies oscillatory in the middle part. The frequency and amplitude of the pattern depends not only on the wavelength/period, but also on the length, mass and rigidity of the structure. The longer the wave is, the longer are the deformations experienced by the sheet. Shown in figures 3 and 4, both the GN solution and linear solutions, obtained by eigen-expansion method, exhibit the same behaviour and are in a nearly perfect agreement. In addition, figure 4 complements the comparisons with theoretical results of the linear theory by providing the vertical displacement amplitudes measured through the laboratory experiments of Kohout et al. [8]. Overall, the GN results are in close agreement with the laboratory measurements and the theoretical results. The agreement is better for longer-wave periods. For more comparisons and discussion of wave interaction with single and multiple deformable sheets of various properties and in various wave conditions, the reader is referred to [22].

Ren et al. [19] investigated the wave-induced drift motion of a small rigid box by use of the SPH method and through laboratory experiments. This study is used here for comparison purposes. Figure 5 shows the horizontal trajectory of the elastic sheet, under the effect of waves of different height ($H = 0.1$ and $H = 0.25$), predicted by the present approach, and compares it with the results of Ren et al [19] for the rigid plate of the same dimensions. It should be

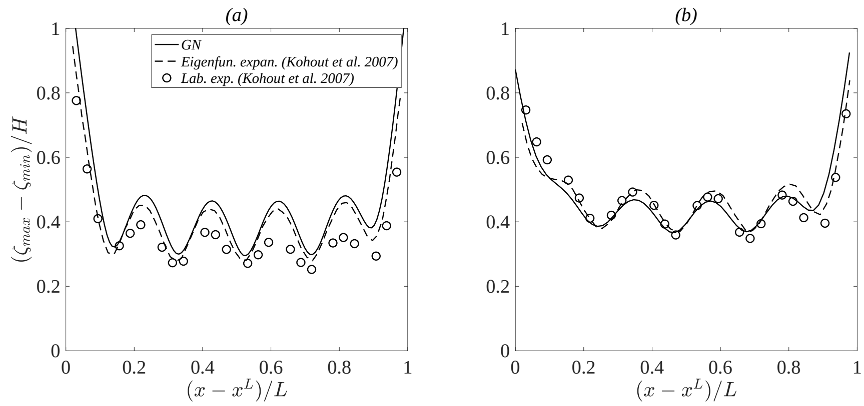

Figure 4. Comparisons of deformation heights of the sheet ($L = 13.3$, $m = 0.02$, $D = 0.37$) under the action of regular waves of periods (a) $T = 4.8$ and (b) $T = 5.7$ without current.

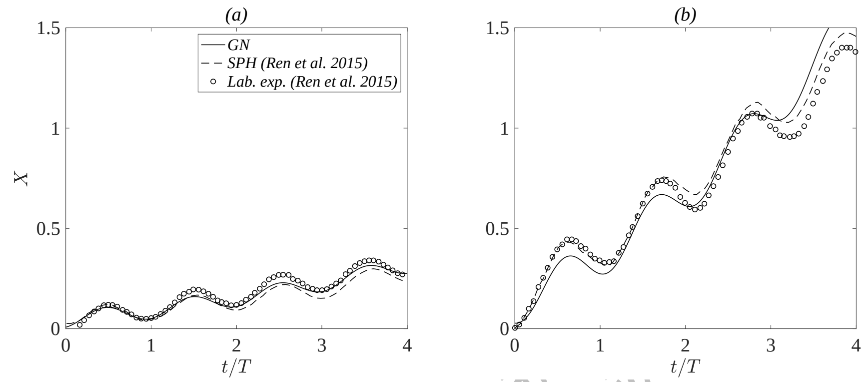

Figure 5. Comparisons of time series of horizontal trajectories of a freely floating sheet ($L = 0.75$, $m = 0.25$, $D = 1$) under the action of regular waves of period $T = 6$ and heights (a) $H = 0.1$ and (b) $H = 0.25$ without current.

noted here that a small elastic sheet in waves behaves as a rigid plate. Furthermore, as it will be shown below, the rigidity parameter has little to no effect on the drift response of the sheet if the wavelength is much longer that the length of the sheet. Figure 5 demonstrates that GN model captures properly the horizontal motion of the floating sheet: for relatively low-amplitude waves ($H = 0.1$), surge and drift motions of the plate predicted by both GN and SPH models are in good agreement with the laboratory measurements; for relatively larger amplitude waves ($H = 0.25$), the GN model slightly underestimates the surge amplitude compared to the results of Ren et al. [19], though predicts the same net drift speed. Some small differences between results is to be expected for larger waves, given the box-shape of the object considered in the study of [19], and its small size when compared to the wavelength. Consideration of such a small object in our model requires extremely small ratio between the grid and time steps, namely in this particular case $\Delta x = 0.15$, $\Delta t = 0.001$ were chosen.

When the relative size of a freely floating body is very small compared to the wavelength, the drift motion of the body may be approximated by the motion of the fluid particles, located at the free surface. For plane progressive waves in a fluid of finite depth, the position of the fluid particles can be defined in Lagrangian coordinates as, see e.g. [51],

$$x(t) = x_0 - \frac{H}{2}\frac{\cosh k(y_0+1)}{\sinh k}\sin(kx_0 - \omega t) + \frac{H^2}{4}\frac{\cosh 2k(y_0+1)}{\sinh k} + O(H^3), \tag{3.1}$$

$$y(t) = y_0 + \frac{H}{2}\frac{\sinh k(y_0+1)}{\sinh k}\cos(kx_0 - \omega t) + O(H^3), \tag{3.2}$$

where (x_0, y_0) is the initial position of the fluid particles and $O()$ refers to the order of the remaining terms. Wave frequency ω is related to the wavenumber k through the linear dispersive relation $\omega^2 = k \tanh k$. Note, that equations (3.1)–(3.2) and dispersive relation are presented here in dimensionless form by use of the water depth h as the length scale. In linear theory, the individual fluid particles on the water surface $(y_0 = 0)$ rotate clockwise along elliptical orbits with semi-axes $H \coth(k)/2$ and $H/2$. The nonlinear feature of the plane progressive waves is the mean drift of fluid particles in direction of wave propagation, as was pointed out by Stokes [6], and is accounted for by the second-order term in equation (3.1). Stokes' expression for the mass-transport velocity of fluid particles on the water surface is written in dimensionless form as:

$$U_s = \frac{H^2}{4}\left(\frac{\omega k \cosh 2k}{2\sinh^2 k} - \frac{\omega}{2}\coth k\right). \tag{3.3}$$

The first term in equation (3.3) is the classical Stokes' drift [6], whereas the second term is the return flow that ensures a net zero depth integrated mean flow [52]. Formula (3.3) is commonly used to estimate qualitatively the drift motion of freely floating small objects in waves, see e.g. [49,53].

In the next section, the time-averaged horizontal velocities of the sheets, predicted by the GN model will be compared with Stokes drift speed given by formula (3.3). The comparisons will show (shown in figures 13 and 14 below, which will be discussed in greater details) that the velocities, calculated by both approaches, exhibit a similar trend. The agreement is good for long waves, which means that the sheet interacting with the long waves, drifts with about the same speed as the fluid particles at the contact surface would move without the body. The agreement is better for lighter and less rigid sheets, which is in line with the assumptions made in obtaining equation (3.3). The differences in the drift speeds predicted by the GN model and Stokes' formula are attributed to the short wave region where Stokes' drift speed increases exponentially, but the floating sheet on the contrary reduces its drift speed due to intensified wave reflection. We will revisit this in the next section.

4. Wave-sheet interaction

As a result of wave- and current-induced loads, a deformable ice sheet floating freely on the water surface moves with a time-averaged drift speed in the direction of wave propagation. This is confirmed by numerous computational simulations, based on slope-sliding model [5,16], SPH method [19] or linear potential theory [49], as well as by experimental observations [17,53,54]. Thereby, the process of wave and current interaction with floating elastic sheet include both elastic bending and translational motion. The former response in the wave-current-structure interaction problem has been discussed in the literature, while the latter (drift motion) remains unexplored. In this analysis, we study the wave- and current-induced deformation and drift motion of elastic sheets and estimate the contribution of the free drift on the dynamic responses. We will consider here two types of floating sheets: (i) *fixed sheet*, is a deformable sheet which can undergo vertical deflections, but is restrained from moving horizontally; (ii) *free sheet*, is a deformable sheet which differs from the fixed sheet by its ability to move freely in horizontal direction, i.e., to drift. In this section, the interaction of cnoidal waves with different elastic sheets without current $(U_c = 0)$ will be investigated by a parametric study. The combined action of wave and uniform current on the floating elastic sheet will be considered in the next section.

Figure 6 shows a free sheet in interaction with the incident wave at three successive time moments. Velocity field (u, v) and pressure distribution $p(x, y)$ in the flow domain are also

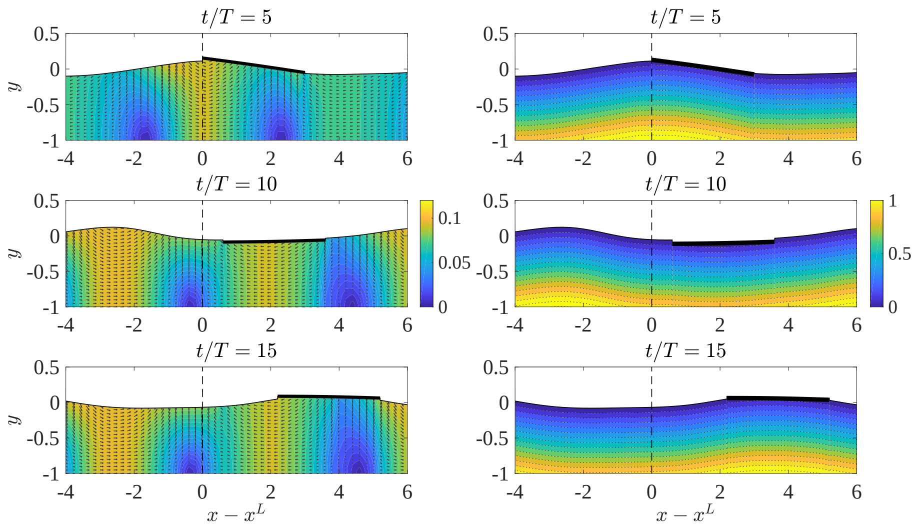

Figure 6. Snapshots of cnoidal wave ($H=0.2$, $\lambda/L=3$, $U_c=0$) interaction with a free sheet ($L=3$, $m=0.1$, $D=1$) at three different time moments. Left column: vectors and dimensionless magnitude of fluid particle velocity; right column: dimensionless fluid pressure. Vertical dashed line indicates the initial position of sheet's leading edge.

presented in the figure. The fluid particles move faster under the wave crests and slower under the wave troughs, the pressure is linearly distributed from the free surface down to the bottom. As seen from figure 6, the sheet bends elastically and drifts with the wave train at the same time, causing the disturbance to the surrounding fluid and breaking the regular character of the fluid velocity distribution.

Figure 7 (a) shows the horizontal trajectories of the drift motion of the free sheet for two incident wave heights. The plots demonstrate the oscillatory motion of the sheet with gradual displacement to the right. The trajectory curve can be decomposed into the sum of translational motion (drift) and periodic oscillations (surge), i.e., $X(t)=X^d(t)+X^s(t)$. Here X^d is the best-fitting trend line of the trajectory curve and X^s is the residual oscillatory signal, see figure 7. The net drift speed U^d and surge oscillation height H^s are then defined as the slope of the trend line X^d and oscillation height of the periodic signal X^s, respectively.

In subsequent analysis, we will be studying the interplay between the drift motion indicators, such as surge oscillation height H^s and net drift speed U^d, and input parameters of the problem, including the wavelength λ, wave height H, sheet length L, unit mass m and rigidity D. In linear theory, the surge amplitude of the freely floating small plate under the action of comparatively long wave of amplitude A tends to the value $A/\tanh kh$, where h is the depth of the fluid [17]. This value corresponds to semi-axis of the elliptic trajectory of fluid particles on the water surface, discussed in the previous section. Therefore, in what follows, the surge oscillation height H^s and net drift speed U^d will be presented in normalized form using $H/\tanh(k)$ and $H\omega/\tanh(k)$ as dimensionless reference values, respectively. In this study, wave condition parameters are selected to cover a range from linear ($H=0.05$, $\lambda=30$) and nonlinear wave conditions ($H=0.15$, $\lambda=3$) with the wave steepness Ak varying from 0.005 to 0.2, respectively. We choose two distinctive sheet sizes, namely $L=3$ and $L=30$, in order to investigate the drift problem in a wide range of plate length to wavelength ratio λ/L, both below and above unity.

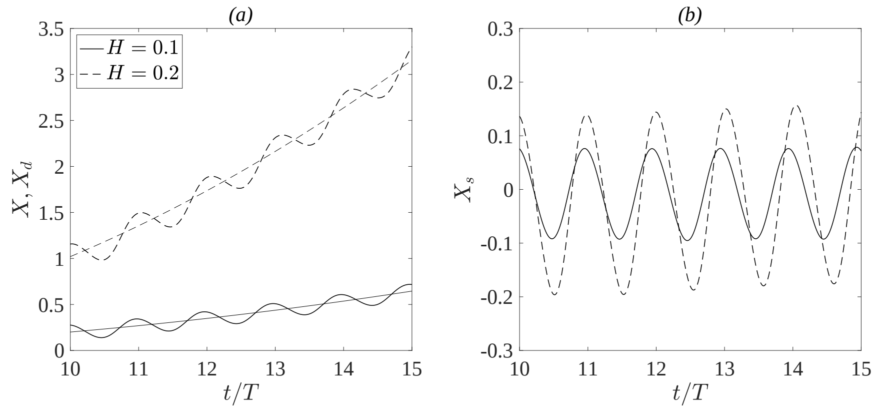

Figure 7. Time series of (a) horizontal trajectory with the best fitting trend lines and (b) pure surge oscillation of a free sheet $(L = 3, m = 0.1, D = 1)$ under the action of cnoidal waves $(\lambda/L = 3)$ of different heights H without current.

(a) Effects of wave conditions

Figure 8 demonstrates how the drift motion changes the wave field around the elastic sheet. The figure shows surface elevation time series at a gauge located one wavelength upwave of the floating sheets, considering both fixed and free sheets for two wavelength conditions. For the fixed sheet case, the wave field retains the regular profile of the incident wave. Compared to its fixed counterpart, the free sheet causes the surface elevation modulation by slowly-varying envelope. This is in line with the observations of Nelli et al. [24], who performed laboratory experiments on moored and freely floating plastic plates under the action of short waves in deep water. As discussed by Nelli et al. as well, the modulations are because the reflection source moves away from the gauge, i.e. the effect of drift. Shown in figure 8, the length of the envelope grows with increase in the incident wavelength.

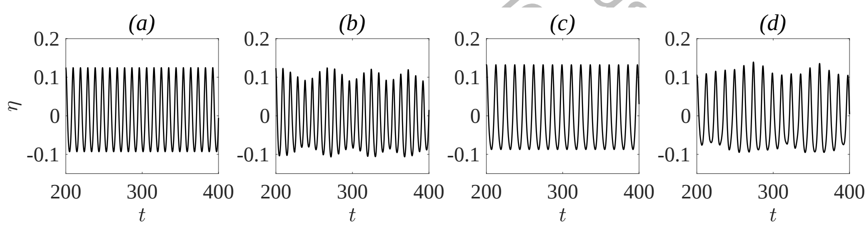

Figure 8. Time series of surface elevation at the gauge located one wavelength upwave of the (a,c) fixed and (b,d) free sheet ($L = 3$, $m = 0.1$, $D = 1$). Cnoidal wave conditions without current: (a,b) $\lambda/L = 3$, $H = 0.2$; (c,d) $\lambda/L = 4$, $H = 0.2$.

Figure 9 shows time series of the horizontal trajectory of a freely floating sheet, its horizontal velocity and wave-induced horizontal force for two cnoidal wave lengths. As it may be expected, the oscillation periods of trajectory, velocity and force correspond to the period of the incoming wave. Comparing the two wave cases in figure 9, we observe that the shorter wave causes larger drift per cycle, accelerates it to a larger speed, but induces smaller surge oscillations. The short and long wave cases differ not only in magnitude of positive and negative velocities and forces, but what is more crucial, in their duration, and this results in different drift behaviour. Surge motion of the sheet under the long wave is characterized by an abrupt displacement on the wave crest and more gradual recurrence motion on the trough. In the long wave regime, the horizontal positive and negative forces are in balance so that the sheet undergoes extensive surge with little horizontal displacement, i.e., there is little drift for longer waves.

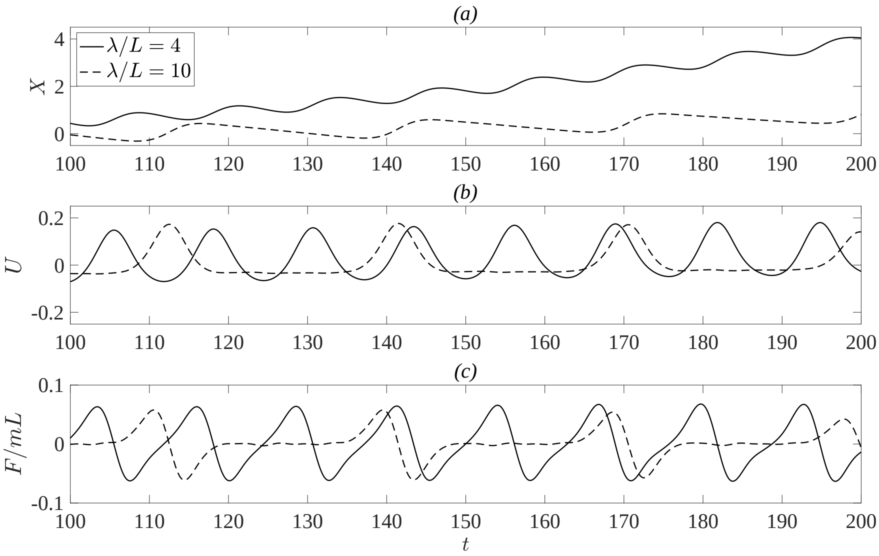

Figure 9. Time series of (a) horizontal trajectory, (b) horizontal velocity, and (c) horizontal force for a free sheet ($L=3$, $m=0.1$, $D=1$) under the action of cnoidal waves ($H=0.2$) of different lengths λ without current.

In figure 10, the normalized surge oscillation height $H^s \tanh(k)/H$ and net drift speed $U^d \tanh(k)/H\omega$ as functions of wavelength to sheet length ratio λ/L are given for cnoidal waves of different heights H. From figure 10, and other figures that will follow, it is observed that sheet's drift motion is strongly affected by the incident wave length. Figure 10 (a) demonstrates that surge response exhibits the growing trend with sharp increase in the short wave region. And in the long wave limit the normalized surge oscillation height approaches the asymptotic value close to unity. The same growth of surge amplitude with incident wavelength has been observed for floating rigid and elastic plates both in linear theory and experiments, see [16,17,49].

The effect of wave nonlinearity can be seen in figure 10 (a). When wavelength is comparable to the size of the sheet, the dimensionless surge plots are insensitive to the change in wave height parameter, indicating that surge oscillation depends linearly on the wave height. Nevertheless, the long wave limiting trends of surge plots corresponding to larger waves start to deviate from the value $H/\tanh(k)$, specific to the linear theory. The second-order character of the drift motion is also illustrated by the plots of the net drift speed in figure 10 (b). The net drift speed, normalized by the incoming wave height, increases with larger wave heights. It is concluded that superfluous part of the wave energy carried by high-amplitude waves results in accelerating the floating sheet to a greater speeds. Hence, in contrast to linear waves, nonlinear waves result in smaller surge and larger drift.

Figure 10 (b) shows that, on the short-wave side to the left of point $\lambda/L \approx 2.5$, the net drift speed increases continuously with wavelength, reaches a maximum at $\lambda/L \approx 2.5$ and then decreases monotonically to zero for longer waves. This corresponds qualitatively to the drift behaviour, predicted by the empirical formula of Harms [54] given for a rectangular-slab ice floe model. According to Harms, the point of maximum net drift speed is where the sheet experiences the transition from short-wave to long-wave drift behaviour. As seen in figure 10 (a), at this transition point the surge oscillation height approaches the maximum and reduces its slope.

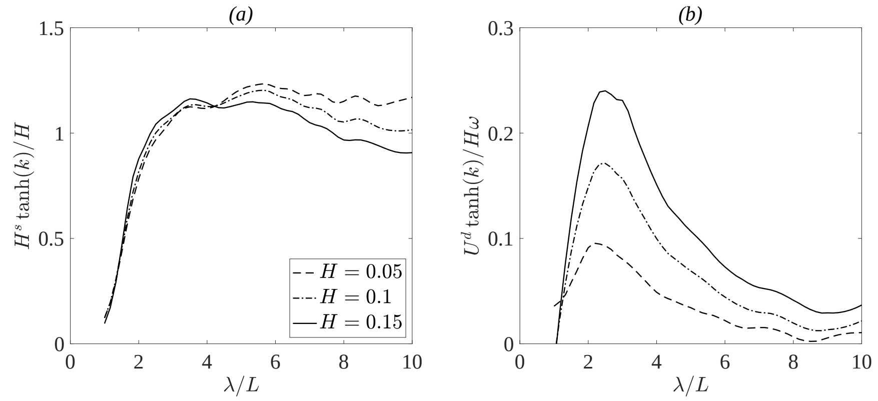

Figure 10. (a) Surge oscillation height and (b) net drift speed of a freely floating sheet ($L = 3, m = 0.1,\ D = 1$) under the action of cnoidal waves of different heights H without current.

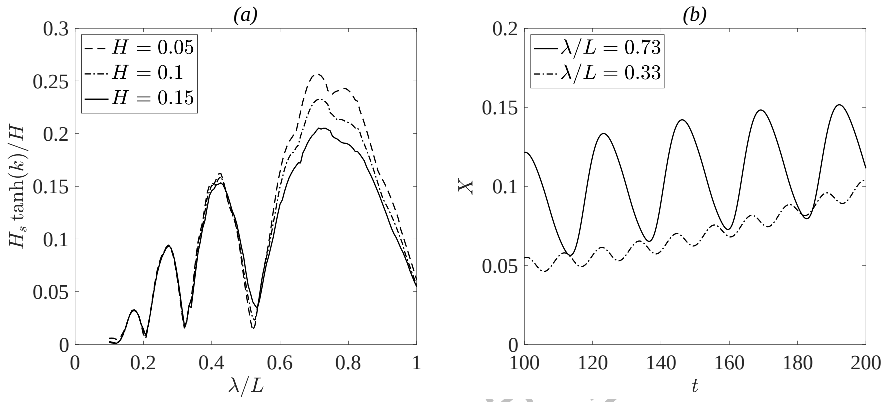

Figure 11. (a) Surge oscillation height of a freely floating sheet ($L = 30$, $m = 0.1$, $D = 1$) under the action of cnoidal waves of different heights H without current. (b) Time series of horizontal trajectories of the same sheet under the action of cnoidal waves ($H = 0.1$) of different lengths without current.

When the sheet is long compared to the incoming wavelength, it experiences little net drift, such that the horizontal motion is limited mainly to surge oscillations. For very small ratios of λ/L, surge oscillation height, apart from the growing trend, has local minimums at the points $\lambda/L \approx 1/2, 1/3, 1/4$, when integer number of waves can be located under the sheet surface, see figure 11. These minimums can be characterized as stagnation zones, where the sheet experiences both little drift and small surge. The peaks between these stagnation points correspond to the resonance regimes, when surge oscillation is comparatively large. Figure 11 illustrates the difference in drift responses of the long sheet to the waves from different regimes. With increase in sheet length new stagnation and resonance regimes occur.

(b) Effects of sheet properties

The effects of sheet's rigidity and mass (draft) parameters on the wave-induced surge and drift are studied here. Figure 12 shows time series of the horizontal trajectories and horizontal forces acting on the elastic sheets of different unit masses m (or draft d, given that volume and density of the sheet are constant). According to figure 12 (a), for the given wavelength, the sheet with larger

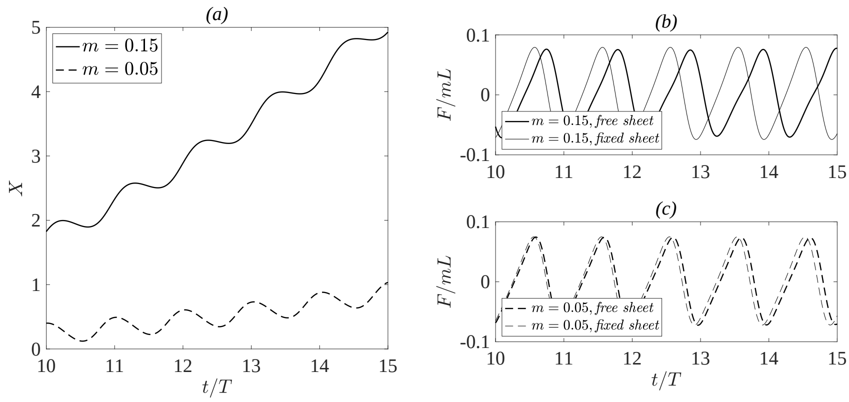

Figure 12. Time series of the (a) horizontal trajectory of freely floating sheets and (b, c) horizontal force on freely floating and fixed sheets ($L = 3$, $D = 1$) of different unit mass m under the action of a cnoidal wave ($\lambda/L = 3$, $H = 0.2$) without current.

unit mass drifts faster. The heavier sheet exhibits larger surge response with elongated period of oscillation, but with almost the same oscillation height. Compared to the force exerted on the fixed elastic sheet, the force on the freely floating sheet has constantly growing period of oscillations, shown in figure 12 (b,c), which is due to the horizontal motion of the sheet relative to the wave train. The difference in the periods of the wave forcing grows faster with increase in the mass parameter m. In fact, heavier sheet has larger contact surface with the fluid and consequently interacts with the surrounding flow more intensely.

Figures 13 and 14 present the normalized surge oscillation height H^s and net drift speed U^d against the wavelength to plate length ratio λ/L for the freely floating sheet of various unit masses m and rigidities D. Figure 13 shows that with increase in the mass parameter m the drift response of the sheet increases proportionally: both in surge and net drift. Still, in the short wave region, neither surge motion nor drift movement of the sheet are not influenced by the mass parameter m. The net drift speed depends on the mass of the sheet in such a way that heavier sheet reaches maximum drift speed at a greater wavelength. From figure 14 it follows that the rigidity parameter D has little to no effect on surge motion of the sheet, but has significant influence on the net drift speed. Sheet with larger rigidity drifts faster and the point of maximum drift speed shifts to the left (to the shorter waves) with an increase in the rigidity parameter. In the long wave limit, rigidity plays no role in the drift response of the floating body. Thus, under long-wave conditions, floating elastic sheet and rigid plate of the same mass and dimensions should exhibit similar drift behaviour. This observation justifies the comparisons with rigid plate case in section 3.

When wavelength to sheet length ratio λ/L is small (the sheet is long), increase in the mass parameter m leads to increase in surge response of the sheet. Seen in figure 15, for larger mass parameter the surge oscillation plots are slightly compressed with subsequent shift in the extremum points. The rigidity parameter appears to have little to no effect on the surge response of the sheet regardless of the incoming wavelength.

Figure 16 presents the plots of the normalized net drift speed U^d against sheet unit mass m and rigidity D for three representative wave regimes, $\lambda/L = 2, 3, 4$, around the point of the maximum drift speed, previously observed in figures 10, 13 and 14. Figure 16 (a) demonstrates that the net drift speed grows almost linearly with an increase in the mass parameter with coefficient of proportionality dependent on the incoming wavelength. As regards to rigidity, the net drift speed reveals asymptotic dependence. Figure 16 (b) shows that the net drift speed grows rapidly at small rigidities, approaching the maximum, determined by the incoming wavelength and mass parameter of the sheet, asymptotically. In other words, for a given sheet mass parameters and wave conditions, there is a critical value of the drift speed that cannot be exceeded by the

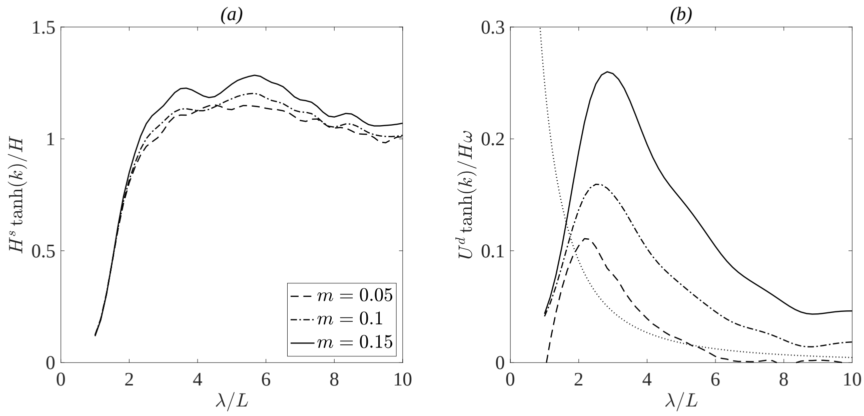

Figure 13. (a) Surge oscillation height and (b) net drift speed of a freely floating sheet ($L = 3$, $D = 1$) of different unit mass m under the action of cnoidal waves of height $H = 0.1$ without current. Dotted line indicates Stokes' drift speed.

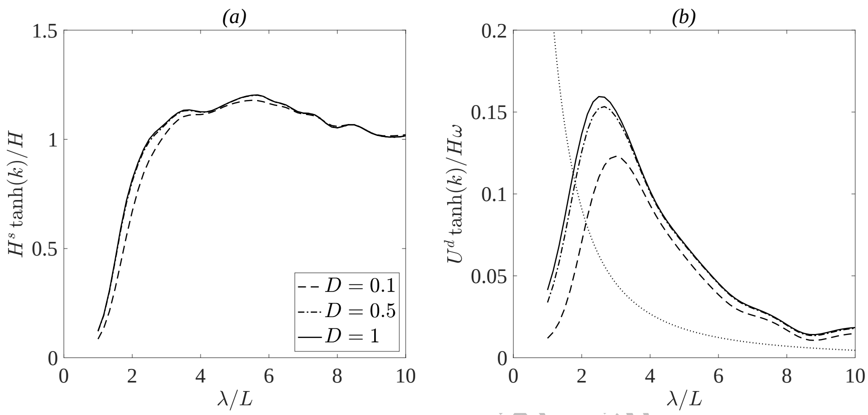

Figure 14. (a) Surge oscillation height and (b) net drift speed of a freely floating sheet ($L = 3, m = 0.1$) of different rigidity D under the action of cnoidal waves of height $H = 0.1$ without current. Dotted line indicates Stokes' drift speed.

freely floating sheet. Indeed, starting from the value $D = 0.5$, increase in rigidity parameter has little to no effect on drift movement of the sheet. The effect of rigidity is less remarkable when wavelength increases. Hence, under the long wave conditions, the drift response of an elastic sheet is approximately equal to the drift response of a rigid plate, regardless of the difference in rigidity. In this case, the rigidity effect is mostly in vertical direction and in the elastic bending of the sheets, and has relatively less influence on the horizontal motion. Further details on the effect of rigidity on the interaction of waves with fixed elastic sheets are discussed in [22].

5. Wave-current-sheet interaction

In real marine conditions, waves usually travel on a current, which could affect the wave propagation speed as well as the wavelength. The phenomenon of wave-current interaction without a floating body has been studied extensively: various theoretical solutions for waves on currents of sheared profiles with non-zero vorticity has been developed and tested in the experiments, see e.g. [55–57]. When the current is uniformly distributed over the water depth, the wave-current interaction may be described by a Doppler shift [58]. Das et al. [59] studied the

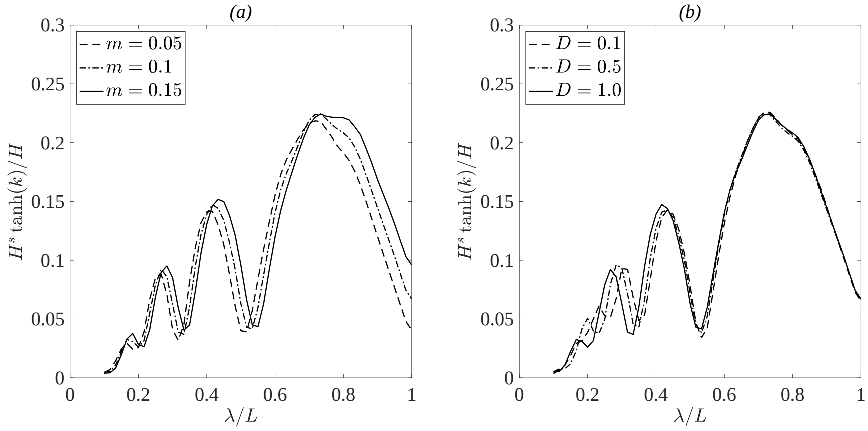

Figure 15. Surge oscillation height of a freely floating sheet of length $L = 30$ with (a) different unit mass m (rigidity $D = 1$) and (b) different rigidity D and (mass $m = 0.1$), under the action of cnoidal waves of height $H = 0.1$ without current.

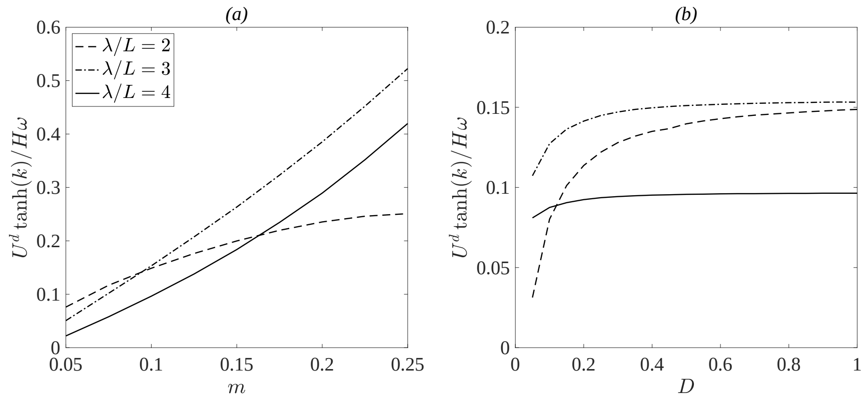

Figure 16. Net drift speed of a free sheet of length $L = 3$ and various mass m and rigidity D under action of a cnoidal wave ($\lambda/L = 2$, $H = 0.1$) without current against its (a) unit mass m for different rigidity D and (b) rigidity D for different unit mass m.

effect of current on wave propagation in the elastic sheet with compressive force and observed the shifting of the blocking points, where the group velocity of the elastic wave goes to zero. In this study, we investigate the combined action of waves and uniform currents on a freely floating elastic sheet located in shallow waters without compressive force. Our goal here is to determine the effect of current on the drift motion of the sheet in the presence of waves.

Initially, two current conditions are considered, equal in speed and opposite in directions. By definition, the wavemaker generates waves travelling with the favourable (or adverse) current, when $U_c > 0$ (or $U_c < 0$) in equation (2.16). The current speed U_c is chosen small relative to the speed of the incident wave ($U_c/c \ll 1$), but similar in magnitude to the orbital motion of fluid particles, see e.g. [56]. This corresponds to real sea conditions, where forcing from tidal currents has been measured and estimated to be negligible when compared to the wave-induced loads [4]. The weak current conditions result in that wave-current-sheet interaction process to occur without wave blocking.

Figure 17 shows wave profiles generated by superposition of a cnoidal wave and uniform current without a floating body, and recorded by a gauge located one wavelength downwave of the wavemaker. According to figure 17, the favourable and adverse currents lead to increase and decrease of the wave elevation, respectively, due to additional fluid mass transferred by the current. Snapshots of surface elevation in figure 17(b) show the variations in the wavelength resulting from the interaction of waves with the current. The influence of a favourable current is found to increase the wavelength, while the opposite occurs in the case of an adverse current.

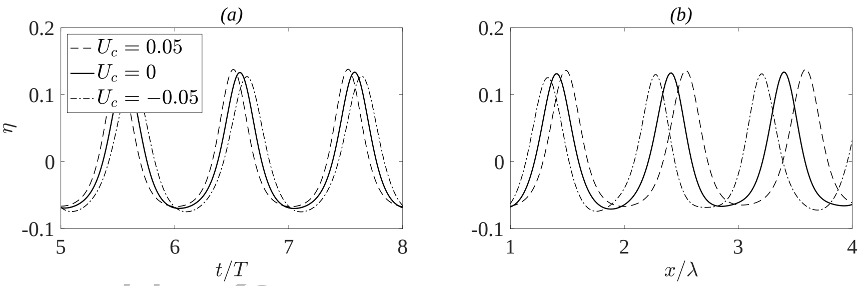

Figure 17. Surface elevation of a cnoidal wave ($\lambda = 15$, $H = 0.2$) with and without current: (a) time series at the gauge located one wavelength downwave of the wavemaker; (b) snapshots at the time moment $t/T = 9.5$.

In figure 18, the drift motion of the floating sheet subject to the combined wave-current loads is presented. The trajectory plots in figure 18 (a) show that the favourable current causes the sheet to move faster when compared to the sheet floating in waves without current, while the adverse current works just the opposite. This is partially due to the effect of the current on the incoming wave height, as it was shown in figure 17, which affects the wave forcing on the floating sheet. It is observed that the segments of the forward drift motion are inclined at the same angle regardless of the current conditions. At the same time, the segments of the backward drift motion go steeper for adverse current, and more flat if the current is favourable. In other words, in the presence of current, the minimum drift speed changes with current direction, but the maximum drift speed remains invariant. Figures 18 (b-d) demonstrate the effect of current on the velocity field around the free sheet. Compared to the pure wave case, the fluid particles around the sheet floating in waves and current move faster or slower depending on the current direction. It can be seen that the favourable current supress the backward flow and stimulates the flow of fluid particles in the wave direction. The opposite is true for the adverse current. Since the current has influence on the wavelength the distance between the wave packages changes correspondingly.

Figure 19 illustrates the effect of current on drift movement of the floating sheet in a range of wavelengths to sheet length ratios λ/L. As seen in figure 19 (a), the surge oscillations of the sheet is invariant with the presence of current, regardless of its direction and speed. Figure 19 (b) shows that combined action of wave and current results in increase or decrease of the net drift speed, depending on the current direction, in all possible wave regimes. It is observed that while the magnitude of the drift motion increases or decreases with favourable or adverse current, respectively, the behaviour of the responses is invariant for all wavelengths. The same behaviour is observed for waves with different heights (results not presented here for brevity).

Figure 20 shows the variation of the net drift speed of the sheet U^d with the ambient current speed U_c. It is observed that the drift speed grows linearly with increase in the current speed at the same rate regardless of the incoming wavelength. Small deviations from the linear relationship for the largest current speeds is observed and this is attributed to the current speed suppressing the wave-induced motion of water particles (in favourable or adverse direction, depending on the current direction) at such extreme conditions, which results in change of behaviour of the velocity and pressure fields.

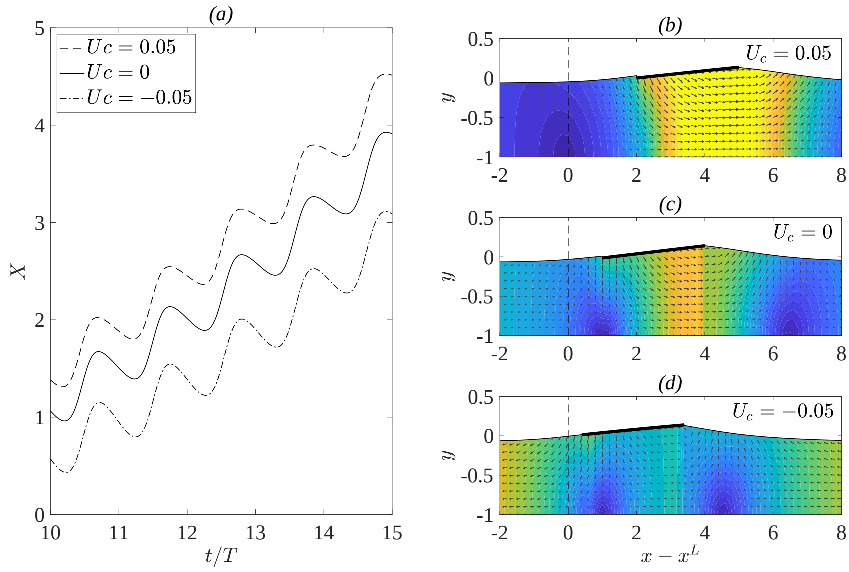

Figure 18. Interaction of a free sheet ($L = 3$, $m = 0.1$, $D = 1$) with a cnoidal wave ($\lambda/L = 5$, $H = 0.2$) with and without current: (a) time series of horizontal trajectory of the sheet; (b,c,d) vectors and dimensionless magnitude of fluid particles velocity at the moment of time $t/T = 9.5$. Vertical dashed line indicates the initial position of sheet's leading edge.

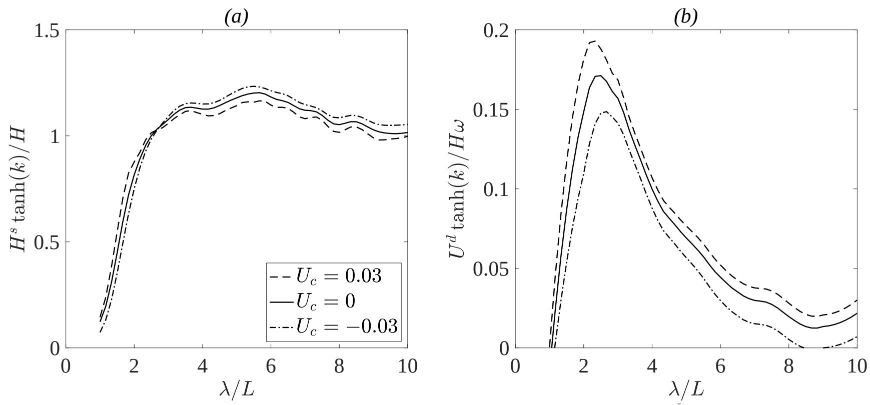

Figure 19. (a) Surge oscillation height and (b) net drift speed of a freely floating sheet ($L = 3$, $m = 0.1$, $D = 1$) under the action of cnoidal waves ($H = 0.1$) with and without current.

6. Conclusions

In this paper, the nonlinear two-dimensional model of interaction of waves and current with a freely floating deformable sheet without overwash is presented. The model is developed based on the coupled Level I GN equations and thin plate theory, and the calculations are performed by use of a finite difference technique. We proposed here an effective analytical and numerical algorithm without moving or nonuniform spatial grids, which accounts for the two-way interaction between the fluid and the structure, including both elastic deformation of the body and flow-induced drift motions. The model shows close agreement with available laboratory measurements and numerical data for elastic deformation and drift movement of floating plates. We estimate the

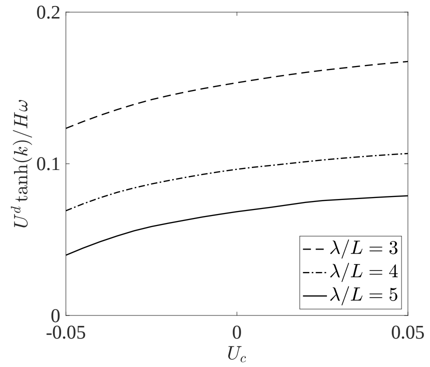

Figure 20. Net drift speed against current speed U_c for a free sheet ($L = 3$, $m = 0.1$, $D = 1$) under combined action of current and cnoidal waves ($H = 0.1$) of different lengths λ/L.

indicators of drift movement by a comprehensive study with various sheet properties, wave parameters and current speeds.

Some of the conclusions are summarized as follows: (i) the ratio of wavelength to the sheet length is an important factor governing the wave-induced drift of the floating sheet: in particular, for wavelength roughly equal to 2.5 sheet lengths, the sheet drifts with maximum speed; (ii) under the action of very long waves, the sheet drifts with a minimum speed and oscillates around the equilibrium position with the maximum amplitude, equal to the amplitude of fluid particle oscillation on the free surface; (iii) the fixed sheet experiences greater impact from the incoming wave than the freely floating sheet, which means that by applying different fixations on the floating sheet, its damping features can be manipulated; (iv) more rigid and heavier sheets drift faster than less rigid and lighter sheets, and the drift speed depends linearly on mass and nonlinearly on rigidity; (v) the current has stimulating and suppressing effects on the drift of floating sheets depending on the current direction.

The results obtained in this study provide an insight to predicting the ice formation in polar regions, their motion and effect on the flow field, safe marine operations and dynamic positioning of solitary and multiple floating offshore structures. Information on kinematic response of the floating object in waves is important for design of the mooring systems. Mechanisms of the wave-absorbing devices can be improved by taking advantage of both vertical and horizontal oscillations of its floating elastic components. And thus more effective collection of the wave energy can be achieved.

In nature, multiple floating sheets, like collection of ice floes, are more likely to occur. The presence of multiple objects impose more complicated fluid-structure interaction conditions, and energy reflection and transition, which opens new possibilities for analysis and interesting physical effects. This will be the subject of the part II paper.

References

1. Serreze MC, Holland MM, J. S. 2007 Perspectives on the Arctic's shrinking sea-ice cover. *Science* **315**, 1533–1536.
2. Squire VA. 2011 Past, present and impendent hydroelastic challenges in the polar and subpolar seas. *Phil. Trans. R. Soc. A* **369**, 2813–2831.
3. Alberello A, Bennetts L, Heil P, Eayrs C, Vichi M, MacHutchon K, Onorato M, Tofolli A. 2020 Drift of pancake ice floes in the winter Antarctic marginal ice zone during polar cyclones. *J. Geophys. Res.: Oceans* **125**, 1–16.
4. Sutherland P, Dumont D. 2018 Marginal ice zone thickness and extent due to wave radiation stress. *J. Phys. Oceanography* **48**, 1885–1901.
5. Shen HH, Ackley SF. 1991 A one-dimensional model for wave-induced ice-floe collisions. *Ann. Glaciol.* **15**, 87–95.
6. Stokes GG. 1847 On the theory of oscillatory waves. *Trans. Cambridge Phil. Soc.* **8**, 441–455.
7. Faltinsen OM, Locken AE. 1980 Slow drift oscillations of a ship in irregular waves. *Modelling, Identification and Control* **1**, 195–213.
8. Kohout AL, Meylan MH, Sakai S, Hanai K, Leman P, Brossard D. 2007 Linear water wave propagation through multiple floating elastic plates of variable properties. *J. Fluids Struct.* **23**, 649–663.
9. Koo W, Kim MH. 2004 Freely floating-body simulation by a 2D fully nonlinear numerical wave tank. *Ocean Eng.* **31**, 2011–2046.
10. Jiao LL, Greco M, Faltinsen OM. 2009 Global hydroelastic analysis of pontoon-type VLFS. *Proceedings of the ASME 2009 28th International Conference on Ocean, Offshore and Arctic Engineering, Honolulu, Hawaii, USA.* pp. 1–9.
11. Wehausen JV. 1971 The motion of floating bodies. *Annu. Rev. Fluid Mech.* **3**, 237–268.
12. Grue J, Palm E. 1993 The mean drift force and yaw moment on marine structures in waves and current. *J. Fluid Mech.* **250**, 121–142.
13. Chen XB. 2007 Middle-field formulation for the computation of wave-drift loads. *J. Eng. Math.* **59**, 61–82.
14. Rumer RR, Crissman R, Wake A. 1979 Ice transport in Great Lakes. *Water Resources and Environmental Engineering Research Report 79-3. Great Lakes Environmental Research Laboratory, National Oceanic and Atmospheric Administration, US Department of Commerce, Ann Arbor, MI.*
15. Marchenko AV. 1999 The floating behaviour of a small body acted upon by a surface wave. *J. Appl. Math. Mech.* **63**, 471–478.
16. Meylan MH, Yeiw LJ, Bennetts LG, French BJ, Thomas GA. 2015 Surge motion of an ice floe in waves: comparison of a theoretical and an experimental model. *Ann. Glaciol.* **56**, 155–159.
17. Yiew LJ, Bennets LG, Meylan MH, French BJ, Thomas GA. 2016 Hydrodynamic responses of a thin floating disk to regular waves. *Ocean Modelling* **97**, 52–64.
18. Hu C, Kashiwagi M. 2009 Two-dimensional numerical simulation and experiment on strongly nonlinear wave-body interactions. *J. Mar. Sci. Technol.* **14**, 200–213.
19. Ren B, Ming H, Dong P, Wen H. 2015 Nonlinear simulations of wave-induced motions of a freely floating body using WCSPH method. *Appl. Ocean Res.* **50**, 1–12.
20. Weber JE. 1987 Wave attenuation and wave drift in the marginal ice zone. *J. Phys. Oceanogr.* **17**, 2351–2361.
21. Law AWK. 1999 Wave-induced surface drift of an inextensible thin film. *Ocean Eng.* **26**, 1145–1168.
22. Kostikov V, Hayatdavoodi M, Ertekin RC. 2021 Hydroelastic interaction of nonlinear waves with floating sheets. *Theor. Comput. Fluid Dyn.* **35**, 515–537.
23. Nelli F, Bennetts L, Skene D, Toffoli A. 2020 Water wave transmission and energy dissipation by a floating plate in the presence of overwash. *J. Fluid Mech.* **889**, 1–20.
24. Nelli F, Bennetts L, Skene D, Monty J, Lee J, Meylan M, Toffoli A. 2017 Reflection and transmission of regular water waves by a thin, floating plate. *Wave Motion* **70**, 209–221.
25. Green AE, Naghdi PM. 1976a A derivation of equations for wave propagation in water of variable depth. *J. Fluid Mech.* **78**, 237–246.
26. Green AE, Naghdi PM. 1976b Directed fluid sheets. *Proc. R. Soc. Lond. A.* **347**, 447–473.
27. Kim JW, Ertekin RC. 2000 A Numerical Study of Nonlinear Wave Interaction in Irregular Seas: Irrotational Green-Naghdi Model. *Marine Structures* **13**, pp. 331–348.
28. Kim JW, Bai KJ, Ertekin RC, Webster WC. 2001 A derivation of the Green-Naghdi equations for Irrotational Flows. *J. Engineering Mathematics* **40**, pp. 17–42.

29. Ertekin RC, Hayatdavoodi M, Kim JW. 2014 On some solitary and cnoidal wave diffraction solutions of the Green-Naghdi equations. *Applied Ocean Research* **47**, pp. 125–137.
30. Zhao BB, Zhang TY, Wang Z, Duan WY, Ertekin RC, Hayatdavoodi M. 2019 Application of three-dimensional IGN-2 equations to wave diffraction problems. *J. Ocean. Eng. Mar. Energy* **5**, 351363.
31. Shields JJ, Webster WC. 1988 On direct methods in water-wave theory. *J. Fluid Mech.* **197**, 171–199.
32. Zhao BB, Ertekin RC, Duan WY, Hayatdavoodi M. 2014 On the steady solitary-wave solution of the Green–Naghdi equations of different levels. *Wave Motion* **51**, 1382–1395.
33. Zhao BB, Duan WY, Ertekin RC, Hayatdavoodi M. 2015 High-level Green–Naghdi wave models for nonlinear wave transformation in three dimensions. *Journal of Ocean Engineering and Marine Energy* **1**, 121–132.
34. Webster WC, Zhao BB. 2018 The development of a high-accuracy, broadband, Green–Naghdi model for steep, deep-water ocean waves. *Journal of Ocean Engineering and Marine Energy* **4**, 273–291.
35. Ertekin RC, Webster WC, Wehausen JW. 1986 Waves caused by a moving disturbance in a shallow channel of finite width. *J. Fluid Mech.* **169**, 275–292.
36. Timoshenko SP, Woinowsky-Krieger S. 1959 *Theory of plates and shells*. McGraw-Hill, NY.
37. Barman SC, Das S, Sahoo T, Meylan MH. 2021 Scattering of flexural-gravity waves by a crack in a floating ice sheet due to mode conversion during blocking. *J. Fluid Mech.* **916**, 1–28.
38. Ertekin RC. 1984 Soliton generation by moving disturbances in shallow water: theory, computation and experiment. *PhD thesis, University of California at Berkeley.*
39. Naghdi PM, Rubin MB. 1984 On the squat of a ship. *J. Ship Research* **28**, 107–117.
40. Naghdi PM, Rubin MB. 1981a On the Transition to Planning of a Boat. *J. Fluid Mechanics* **103**, pp. 345–374.
41. Naghdi PM, Rubin MB. 1981b On inviscid flow in a waterfall. *J. Fluid Mechanics* **103**, 375–387.
42. Naghdi PM, Vongsarnpigoon L. 1986a The downstream flow beyond an obstacle. *J. Fluid Mechanics* **162**, 223–236.
43. Naghdi PM, Vongsarnpigoon L. 1986b Steady flow past a sluice gate. *Physics of Fluids* **29**, 3962.
44. Hayatdavoodi M, Ertekin RC. 2015 Wave forces on a submerged horizontal plate – part I: Theory and modelling.. *J. Fluids Struct.* **54**, 566–579.
45. Ertekin RC, Becker JM. 1998 Nonlinear diffraction of waves by a submerged shelf in shallow water. *J. Offshore Mech. Arct.* **120**, 212–220.
46. Neill DR, Hayatdavoodi M, Ertekin RC. 2018 On solitary wave diffraction by multiple, in-line vertical cylinders. *Nonlinear Dynamics* **91**, 975–994.
47. Hayatdavoodi M, Neil DR, Ertekin RC. 2018 Diffraction of cnoidal waves by vertical cylinders in shallow water. *Theor. Comp. Fluid. Dyn.* **32**, 561–591.
48. Bennetts LG, Alberello A, Meylan MH, Cavaliere C, Babanin AV, Toffoli A. 2015 An idealised experimental model of ocean surface wave transmission by an ice floe. *Ocean Modelling* **96**, 85–92.
49. Bai W, Zhang T, McGovern DJ. 2017 Response of small sea ice floes in regular waves: A comparison of numerical and experimental results. *Ocean Eng.* **129**, 495–506.
50. Watanabe E, Utsunomiya T, Kubota A. 2000 Analysis of wave-drift damping of a VLFS with shallow draft. *J. Mar. Struct.* **13**, 383–397.
51. Newman JN. 2017 *Marine hydrodynamics*. The MIT Press Cambridge, Massachusetts London, England.
52. Longuet-Higgins MS. 1953 Mass transport in water waves. *Phil. Trans. Royal Soc. London: A* **245**, 535–581.
53. Huang G, Law AWK, Huang Z. 2011 Wave-induced drift of small floating objects in regular waves. *Ocean Eng.* **38**, 712–718.
54. Harms VW. 1987 Steady wave-drift of modeled ice floes. *J. Waterw. Port Coast Ocean Eng., ASCE* **113**, 606–622.
55. Peregrine DH. 1976 Interaction of water waves and current. *Adv. Appl. Math.* **16**, 9–117.
56. Swan C, James RL. 2001 A simple analytical model for surface water waves on a depth-varying current. *Appl. Ocean Res.* **22**, 331–347.
57. Umeyama M. 2005 Reynolds stresses and velocity distributions in a wave-current coexisting environment. *J. Waterway, Port, Coastal and Ocean Eng.* **131**, 203–212.
58. Fenton JD. 1985 A fifth-order Stokes theory for steady waves. *J. Waterway, Port, Coastal and Ocean Eng.* **111**, 216–234.

59. Das S, Sahoo T, Meylan MH. 2018 Dynamics of flexural gravity waves: from sea ice to Hawking radiation and analogue gravity. *Proc. R. Soc. A.* **474**, 20170223.